TITLE: Apolipoprotein M attenuates doxorubicin cardiotoxicity by regulating transcription factor EB

One sentence summary: Apolipoprotein M attenuates doxorubicin cardiotoxicity by preserving nuclear translocation of TFEB and autophagic flux.

Zhen Guo, PhD[1, *]; Antonino Picataggi, BS[1, *]; Carla Valenzuela Ripoll, MD[1]; Ezhilarasi Chendamarai, PhD[1]; Amanda Girardi[1]; Terrence Riehl, PhD[1]; Hosannah Evie, BS[1]; Juan Villa Torrecilla, PhD[1]; Attila Kovacs, MD[1]; Krzysztof Hyrc, PhD[2]; Xiucui Ma, PhD[1, 3]; Aarti Asnani, MD[4]; Swapnil V. Shewale, PhD[5]; Marielle Scherrer-Crosbie, MD, PhD[5]; L. Ashley Cowart, PhD[6]; John S. Parks, PhD[7]; Abhinav Diwan, MD[1, 3]; Kenneth B. Margulies, MD[5]; Christina Christoffersen, MD, PhD[8]; Michael P. Rettig, PhD[1]; John F. DiPersio, MD, PhD[1]; Ali Javaheri, MD, PhD[1]

1. Washington University School of Medicine, St. Louis, MO 63110
2. Hope Center, Washington University School of Medicine, St. Louis, MO 63110
3. John Cochran VA Medical Center, St. Louis, MO 63106
4. Beth Israel Deaconess, Harvard Medical School, Boston, MA 02115
5. Perelman School of Medicine, University of Pennsylvania School of Medicine/Hospital of the University of Pennsylvania, Philadelphia, PA 19104
6. Virginia Commonwealth University, Richmond, VA 23298 and Hunter Holmes McGuire VA Medical Center, Richmond, VA 23249
7. Wake Forest School of Medicine, Winston-Salem, NC 27104
8. Dept. of Clinical Biochemistry, Rigshospitalet and Dept. of Biomedical Sciences, 2100 Copenhagen, Denmark

*indicates equal contribution

Corresponding author:
Ali Javaheri, MD, PhD
Washington University School of Medicine
CSRB 8818, St. Louis, MO 63105
Phone: 314-273-8367; Fax: 314-362-0186
Email: ali.javaheri@wustl.edu, Twitter: @Alicardsdoc

Conflict of interest: AJ has a pending patent for fusion protein nanodiscs for the treatment of heart failure, receives research funding from AstraZeneca, and owns stock options in DexCom.

Key word: apolipoprotein M, autophagy, anthracycline, TFEB, cardiomyopathy

Abstract

Apolipoprotein M (ApoM) is an apolipoprotein that binds sphingosine-1-phosphate (S1P) and high-density lipoprotein. ApoM, via S1P signaling, is thought to protect cardiomyocytes from apoptosis, and ApoM plasma protein levels are inversely associated with increased mortality risk in human heart failure. Here, using a doxorubicin cardiotoxicity model, we identify ApoM as a novel regulator of myocardial autophagy. Doxorubicin treatment reduces ApoM plasma protein levels in wild-type mice and humans. Hepatic ApoM transgenic overexpression ($Apom^{TG}$) protects mice from reductions in cardiac function observed in littermate controls. Though ApoM did not alter markers of DNA damage, apoptosis, Akt signaling, or fibrosis, ApoM prevented doxorubicin-induced reductions in autophagic flux. In the murine myocardium, doxorubicin reduced the nuclear protein content of transcription factor EB (TFEB), a master regulator of autophagy and lysosomal biogenesis, in control mice but not $Apom^{TG}$ mice. Furthermore, adeno-associated virus 9 mediated knockdown of TFEB reversed the beneficial effects of ApoM on the myocardium, leading to cardiomyopathy and mortality in $Apom^{TG}$ mice. Our studies provide a mechanistic link between ApoM and the autophagy-lysosome pathway in the murine heart. Our clinical observations that reduced ApoM is associated with mortality may be explained by its role in sustaining autophagy.

List of abbreviations

ApoM: apolipoprotein M

ApoA-I: apolipoprotein A-I

HDL: high-density lipoprotein

HF: heart failure

LVEF: left ventricular ejection fraction

S1P: sphingosine-1-phosphate

S1PR1: S1P receptor 1

TFEB: transcription factor EB

Introduction

Chemotherapeutic treatments improve survival for many patients with cancer, but these improvements are offset by increases in therapy-related cardiovascular mortality (1). Anthracyclines, such as doxorubicin, are utilized for the treatment of cancers including breast cancer, leukemia, lymphoma, and sarcoma; however, the use of anthracyclines is limited by acute and chronic cardiotoxicity. Use of doxorubicin remains common, particularly in children, with nearly 50% of children with cancer treated with an anthracycline (2). In children with acute lymphoblastic leukemia treated with at least one dose of doxorubicin, 57% have cardiovascular abnormalities in follow up (3). Although cardiotoxicity is typically clinically defined as a reduction in left ventricular ejection fraction (LVEF), reduced LV mass is a clinical sign that harbors a poor prognosis (4), independent of changes in LVEF or body weight (5).

Long-term, anthracyclines cardiotoxicity can result in heart failure (HF) in approximately 2% of patients, a diagnosis that carries a grave prognosis (6-8). Proposed mechanisms of doxorubicin cardiotoxicity include DNA damage downstream of topoisomerase 2b (9), mitochondrial iron overload (10), and lysosomal injury with decreased nuclear translocation of transcription factor EB (TFEB), a master regulator of autophagy and lysosomal biogenesis (11, 12).

High-density lipoprotein (HDL) has recently been suggested as a potential therapeutic for anthracycline cardiotoxicity and HF (13). In vitro studies indicate that the HDL attenuates cell death due to doxorubicin via sphingosine-1-phosphate (S1P), a bioactive sphingolipid that binds G protein coupled receptors on cardiomyocytes (14). Over 70% of S1P binds directly to the lipocalin apolipoprotein M (ApoM) on HDL particles, while the remainder of S1P is associated with albumin (15). ApoM is secreted primarily by hepatocytes, and is associated with ~5% of HDL particles (and < 2% of low-density lipoprotein particles) (16-18).

ApoM exerts multiple pleiotropic effects, including antioxidant and anti-atherogenic effects (19, 20), regulation of inflammation (21), endothelial protection (15, 21), and cell survival

(22). Hepatocyte-specific overexpression of human *APOM* in mice (*Apom*^{TG}) results in significant increases in plasma ApoM and S1P (18), while ApoM knockout mice (*Apom*^{KO}) exhibit 50% reductions in plasma S1P, with normal amounts of S1P on albumin (15).

Despite our clinical observations that reduced circulating ApoM is associated with increased mortality in HF patients (23), little is known about whether increasing ApoM might improve HF outcomes in vivo. A single standard deviation reduction in ApoM is associated with ~25% increased mortality, independent of the subtype of HF, ischemic heart disease, HDL-C, or apolipoprotein A-I (ApoA-I), the main protein constituent of HDL (23). In the present study, we hypothesized that increasing ApoM would attenuate doxorubicin cardiotoxicity and HF. Using anthracycline cardiotoxicity as a model, we identify that ApoM drives myocardial autophagy and nuclear translocation of TFEB. These studies point towards a novel function of the ApoM/S1P axis in regulating the autophagy-lysosome pathway in the myocardium, and could explain the observed associations between ApoM and HF survival.

Results

Anthracyclines reduce circulating ApoM protein levels

Reduced circulating ApoM protein levels are associated with poorer survival in HF patients (23). Given the known cardiotoxicity caused by anthracyclines (24), we tested whether anthracyclines can reduce ApoM in mice and humans. We found that acute doxorubicin treatment of mice reduces plasma ApoM (**Figure 1, A and B**). Furthermore, we observed concordant decreases in circulating ApoM in breast cancer patients (clinical information shown in **Supplementary Table**) treated with anthracyclines for four cycles (**Figure 1C**).

We therefore sought to investigate how doxorubicin might be reducing ApoM. Surprisingly, doxorubicin treatment increased both hepatic ApoM protein and mRNA abundance (**Supplementary Figure 1, A-C**), suggesting increased hepatic ApoM production. We therefore sought to examine urinary excretion of ApoM after doxorubicin. ApoM could be detected by Western blot in the urine of 2/3 mice treated with doxorubicin (**Supplementary Figure 1D**), but in no other urine samples (0/9). Mechanistically, treatment of human proximal tubular cells acutely with doxorubicin resulted in decreased mRNA expression of megalin (Lrp2) (25), an ApoM receptor critical for ApoM reabsorption from the urine (**Supplementary Figure 1E**). These data suggest that anthracycline treatment reduces circulating ApoM protein levels in mice and humans as a result of anthracycline-induced downregulation of kidney Lrp2 with increased urinary excretion of ApoM.

ApoM attenuates doxorubicin induced mortality and cardiotoxicity

Given the reduction in plasma ApoM caused by doxorubicin, we investigated whether increasing ApoM was sufficient to attenuate cardiotoxicity caused by the drug. In initial studies comparing $Apom^{TG}$ to non-transgenic littermate controls, we modeled cardiotoxicity using high dose, acute treatment with doxorubicin (20 mg/kg IP). In these experiments, we observed increased survival of $Apom^{TG}$ mice within 7 days (**Figure 2A**). $Apom^{TG}$ mice were protected from doxorubicin-

induced reductions in LV mass that occurred in littermate controls (**Figure 2B**). In chronic studies with doxorubicin delivered via tail vein injection (5 mg/kg x 4 doses delivered once per week), we observed reductions in LVEF in littermate controls but not in *Apom*^{TG} mice (**Figure 2C**). We also modeled *Apom*^{TG} mice that were crossed into an *Apom*^{KO} mouse background, to determine whether murine ApoM was required for the effects of human ApoM overexpression. Human ApoM overexpression also suppressed doxorubicin-induced reductions in LV mass that occurred in the *Apom*^{KO} mouse background (**Figure 2D**). Hence, murine ApoM was not required for the beneficial effects of human ApoM against doxorubicin cardiotoxicity. Finally, using a murine model of acute promyelocytic leukemia (26, 27), we observed that doxorubicin treatment (subcutaneous 4 mg/kg x 6 doses) extended survival to a similar degree in *Apom*^{TG} mice compared to littermate controls (**Supplementary Figure 2A**) with a similar degree of blast suppression 2 days after the last dose of doxorubicin (**Supplementary Figure 2B**), indicating that ApoM does not attenuate the anti-leukemic efficacy of doxorubicin in vivo.

ApoM does not alter DNA damage, apoptosis, Akt signaling, or fibrosis in doxorubicin induced cardiotoxicity

We next investigated mechanisms by which ApoM could attenuate doxorubicin cardiotoxicity. First, we examined myocardial γ-H2AX (28) foci as a marker of DNA damage resulting from acute doxorubicin administration (48 hr after one dose, 10 mg/kg), and found no difference in foci in *Apom*^{TG} versus littermate control mice (**Supplementary Figure 3**). As HDL can attenuate apoptosis caused by doxorubicin in vitro (14), we performed anti-caspase 3 immunohistochemistry in myocardial sections from the above mice, and again found no significant differences (**Supplementary Figure 4**). Furthermore, the levels of myocardial anti-caspase 3 staining were relatively modest compared to positive controls obtained from prior closed-chest ischemia reperfusion experiments (29).

Transgenic overexpression of ApoA-I (*Apoa1*^{TG}), the main protein constituent of HDL, attenuates doxorubicin cardiotoxicity via the phosphoinositol-3-kinase/protein kinase B (PI3K/Akt) pathway (13). We confirmed that *Apoa1*^{TG} mice exhibited increased Akt phosphorylation at Ser473; however, we did not observe increased phosphorylation of Akt at Ser473 in *Apom*^{TG} mice (**Supplementary Figure 5, A-D**). Furthermore, evaluation of mitochondrial ultrastructure by electron microscopy did not demonstrate marked qualitative differences in acute or chronic doxorubicin cardiotoxicity models (**Supplementary Figure 6, A and B**), nor was there evidence of reduced fibrosis by Masson's trichrome stain at later timepoints (**Supplementary Figure 7**). Altogether, these studies suggest that ApoM did not attenuate cardiotoxicity in doxorubicin cardiotoxicity by impacting DNA damage, apoptosis, Akt signaling, or fibrosis in the myocardium.

ApoM overexpression prevents doxorubicin-induced autophagic impairment, which is observed in human anthracycline cardiomyopathy

We therefore turned our attention to potential novel effects of ApoM/S1P on autophagy and lysosome dysfunction, both of which have recently been reported in murine models of doxorubicin cardiotoxicity (11, 12). To measure autophagic flux, we performed immunohistochemistry for the autophagy proteins LC3 and p62, an autophagy receptor and substrate, respectively, from myocardial sections of mice treated with vehicle and doxorubicin plus or minus the lysosomal inhibitor chloroquine. Compared to littermate controls, *Apom*^{TG} exhibited intact autophagic flux after doxorubicin, as evidenced by accumulation of LC3 (**Figure 3, A and B**) and p62 (**Figure 3, C and D**) with chloroquine.

Accumulation of insoluble p62 in the myocardium is an indicator of autophagic impairment that occurs in human and murine heart failure (30, 31). We assayed accumulation of insoluble p62 in murine *Apom*^{KO} *Apom*^{TG} mice versus littermate *Apom*^{KO} mice at the same timepoint at which echocardiography was performed (**Figure 2D**). In contrast to doxorubicin-

treated *Apom*^{KO} mice, *Apom*^{KO} *Apom*^{TG} mice exhibited reduced insoluble p62 (**Figure 4, A and B**). To determine whether autophagic impairment occurs in human anthracycline cardiomyopathy, we obtained left ventricular myocardial tissue from patients with a history of heart failure due to anthracycline cardiotoxicity versus donor controls obtained from patients without any known clinical heart failure. Left-ventricular myocardium from anthracycline cardiomyopathy patients exhibited increased insoluble p62 relative to donors (**Figure 4, C and D**), suggestive of impaired autophagy in anthracycline cardiotoxicity.

ApoM regulates myocardial autophagy by preserving nuclear TFEB

Reductions in autophagy due to doxorubicin may be causally related to decreases in nuclear TFEB protein, a transcription factor and master regulator of lysosomal biogenesis. To determine whether ApoM overexpression was also sufficient to preserve nuclear translocation of TFEB, we performed nuclear protein isolation from control and *Apom*^{TG} hearts treated with doxorubicin. ApoM overexpression did not increase nuclear levels of TFEB at baseline. Nevertheless, in contrast to controls, which showed reductions in nuclear TFEB protein levels after doxorubicin, *Apom*^{TG} mice demonstrated preservation of active, nuclear TFEB (**Figure 5, A and B**), as evidenced by preserved levels of the faster migrating, dephosphorylated band that represents active TFEB. To determine whether this could be an acute effect of ApoM administration, we performed plasma transfer from *Apom*^{TG} or *Apom*^{KO} mice to recipient *Apom*^{KO} mice prior to administration of vehicle or doxorubicin (**Figure 5C**). Assessment of TFEB nuclear protein content showed that plasma transfer from *Apom*^{TG} but not *Apom*^{KO} donors could attenuate doxorubicin-induced reductions in nuclear TFEB (**Figure 5, D and E**).

To determine whether TFEB was causally involved in cardioprotection by ApoM, we utilized a strategy of adeno-associated virus 9 (AAV9) short-hairpin RNA-mediated TFEB knockdown (30). Littermate control and *Apom*^{TG} mice were injected with 3.5e11 viral particles of AAV9-shScramble versus AAV9-shTFEB. AAV9-shTFEB transduction resulted in significant

reductions in TFEB mRNA abundance in littermate controls and *Apom*^{TG} mice (**Figure 6A**). Echocardiographic evaluation of mice demonstrated that in contrast to littermate controls, *Apom*^{TG} had significant reductions in heart rate (**Figure 6B**), no significant change in ejection fraction (**Figure 6C**), but significant increases in end-diastolic volume (**Figure 6D**); hence, in contrast to littermate controls, *Apom*^{TG} mice suffered adverse LV remodeling after TFEB knockdown. When a subset of mice were treated with doxorubicin (before we were aware of the echocardiographic results), 2/3 *Apom*^{TG} AAV9-shTFEB mice died after a single dose of doxorubicin (5 mg/kg IP). To determine the effect of TFEB knockdown on autophagy, we performed immunostaining for LC3 in littermate control and *Apom*^{TG} mice above. In comparison to mice transduced with null virus, only *Apom*^{TG} transduced with AAV9-shTFEB exhibited reductions in LC3 foci (**Figure 6, E and F**). Based on the echocardiographic results and the extreme response to doxorubicin, we concluded that TFEB is required for cardioprotection by ApoM.

Cardiomyocyte S1P signaling through S1PR1 regulates myocardial TFEB

ApoM binds the bioactive lipid S1P, which is known to activate S1P receptors expressed on cardiomyocytes. Based on this paradigm and our described effects of ApoM on autophagy and TFEB, we hypothesized that S1P receptors mediate the effect of ApoM on TFEB; however, S1P receptor 1 (S1PR1) signaling has been described to negatively regulate autophagy (32). Therefore, we crossed alpha myosin heavy chain Cre (αMHC-Cre) mice to *S1pr1*$^{flox/flox}$ mice to generate cardiomyocyte-specific S1pr1 knockout mice (*S1pr1*^{CMKO}). Although *S1pr1*^{CMKO} develop cardiomyopathy with aging (33), *S1pr1*^{CMKO} exhibit structurally normal hearts at 7-8 weeks of age (**Supplementary Figure 8**). At this time point, compared to littermate controls, *S1pr1*^{CMKO} exhibited reduced nuclear TFEB content after both vehicle and doxorubicin treatment (**Figure 7, A and B**). The nuclear TFEB protein content in *S1pr1*^{CMKO} was similar to the level in

doxorubicin-treated controls, suggesting that cardiomyocyte S1PR1 may be required for myocardial TFEB activation.

To determine whether inhibition of S1P receptor signaling is required for TFEB activation in *Apom*^{TG} mice, we utilized the S1PR1/3 inhibitor VPC23019 (34). Compared to vehicle treated mice, *Apom*^{TG} mice treated with VPC23019 for 3 days exhibited reduced nuclear TFEB content at baseline (**Figure 7, C and D**), suggesting that S1P signaling mediates the effects of ApoM on TFEB.

Both anthracyclines and other chemotherapeutic drugs activate a lysosomal stress response characterized by loss of lysosomal pH (11) and lysosomal exocytosis, as evidenced by redistribution of lysosomes to the plasma membrane (35). To determine whether an S1P mimetic could attenuate lysosomal injury, we treated neonatal rat cardiomyocytes (NRCMs) with either vehicle or the S1P mimetic FTY720 prior to treatment with doxorubicin, followed by live cell microscopy with Lysosensor DND-160, a pH sensitive ratiometric probe that can be utilized to measure pH in acidified organelles. To harness only the S1P activating effects of FTY720, NRCMs were pre-treated with 25 nM of FTY720 for 5 min prior to washing the cells with PBS and subsequent treatment with low dose doxorubicin. In these experiments, we were careful to treat with low-dose (0.5 μM) doxorubicin for only 4 hr in order to minimize cytotoxic effects of the drug seen with higher doses and longer timepoints. Treatment of NRCMs with doxorubicin resulted in a characteristic pattern of lysosomal exocytosis (**Figure 7, E and F**, top right panel) that was abrogated by pre-treatment with FTY720 (**Figure 7, E and F**, bottom panel). Furthermore, doxorubicin resulted in acute changes in lysosomal pH over 4 hr that were attenuated by pre-treatment with FTY720.

Discussion

Our results indicate that the ApoM/S1P attenuates doxorubicin cardiotoxicity by maintaining nuclear TFEB and preserving autophagic flux. We demonstrate a mechanistic link between ApoM, an HDL-associated apolipoprotein, and autophagy that is mediated by S1P signaling. Our studies therefore demonstrate how cardioprotection by HDL and S1P (36, 37) may be mediated by TFEB, which is a known master regulator of lysosomal function and autophagy. The translational relevance of our studies is highlighted by our novel observations that a) anthracycline treatment reduces plasma ApoM protein levels, b) the ApoM/S1P axis preserves autophagic flux and TFEB nuclear protein levels in the face of doxorubicin, and c) autophagic impairment is a characteristic of doxorubicin cardiomyopathy in humans. These studies offer mechanistic insight into our prior clinical observations showing that reduced circulating ApoM is associated with increased mortality in human HF (23).

We observed that anthracyclines reduce circulating ApoM protein levels in breast cancer patients, and were able to model reductions in ApoM with acute doxorubicin administration in mice. Contrary to our initial hypothesis, doxorubicin did not reduce hepatic ApoM mRNA or protein abundance, suggesting that doxorubicin is unlikely to reduce hepatic ApoM production. However, we were able to detect urinary ApoM excretion in mice after a single dose of doxorubicin, and in vitro evidence suggested that doxorubicin downregulates mRNA abundance of Lrp2 (megalin), a known receptor for ApoM, albumin, and other proteins (25). As reductions in megalin protein levels are implicated in chronic kidney disease and proteinuria, our results offer a potential novel link between anthracycline cardiotoxicity and nephrotoxicity that merits further exploration. Furthermore, given what is known about the associations between reduced ApoM and HF outcomes, the significance of anthracycline-mediated reductions of ApoM and links to reductions in LV mass should also be addressed in future human studies.

What are the mechanisms by which increasing ApoM attenuates doxorubicin cardiotoxicity? We did not observe acute effects on DNA damage, Akt signaling, or caspase-3

levels, arguing that ApoM does not interfere with the upstream effects of doxorubicin on these processes. Instead, we find that ApoM exerts protective effects on the myocardium via S1P-mediated preservation of nuclear TFEB levels. We demonstrate that S1PR1 is required for these effects, as *S1pr1*^{CMKO} exhibit baseline reduction in nuclear TFEB levels. Our findings raise the hypothesis that reduced autophagy and TFEB activity in the *S1pr1*^{CMKO} may be related to the cardiomyopathy these mice develop with advanced age (33). In addition, we show that S1P signaling is required for the effects of ApoM on TFEB, because treatment of *Apom*^{TG} mice with VPC23019, an inhibitor of S1P receptor signaling, decreases nuclear levels of TFEB.

One outstanding question is what pathways downstream of S1P are involved in activation of TFEB. As S1P can activate the adenosine-monophosphate protein kinase (AMPK) pathway (38), and AMPK is known to activate TFEB independently of mammalian target of rapamycin (39), we propose that ApoM/S1P, via S1PR1 and AMPK can activate TFEB.

We find that autophagic impairment is a characteristic of anthracycline cardiomyopathy in humans. Although anthracyclines mediate toxicity via multiple pathways, lysosomes have recently emerged as a critical target of anthracyclines and other anti-neoplastic drugs (11, 12, 35), and have an increasingly recognized role in cardiometabolic disease (40). In humans with anthracycline cardiomyopathy, we demonstrate accumulation of insoluble p62, suggesting that autophagic impairment observed previously in murine models (11) also occurs in humans. Our studies show that ApoM might be an attractive therapeutic strategy, as overexpression of ApoM did not impact the anti-neoplastic efficacy of doxorubicin while protecting against cardiotoxicity and reducing insoluble levels of p62. In addition, since preservation of autophagic flux has been implicated in the pathogenesis of HF more broadly (30, 31), our studies may help explain the broader link between ApoM and HF outcomes.

Our studies add to a growing body of murine and human literature suggesting that apolipoproteins, in particular HDL apolipoproteins, may serve a therapeutic role in HF. Both HDL subclasses and ApoM are associated with HF survival in humans (23, 41), and multiple

rodent studies have focused on the potential benefit of HDL after myocardial infarction, or ApoA-I in HF models. That ApoM is a novel regulator of TFEB and autophagy only underscores the complexity and importance of achieving a careful, mechanistic understanding of these pathways and their therapeutic potential.

Methods

Reagents

Doxorubicin hydrochloride (50 mg) was purchased from United States Pharmacopeia (USP, R11760, Rockville, MD, USA) and dissolved in 20 ml of molecular grade water to get a 2.5 mg/ml stock, which was used in animal and cell experiments. VPC23109 was purchased from Tocris (#4195, Minneapolis, MN, USA) and dissolved in acidified DMSO (5% 1N HCl in DMSO) to 5 mM. For animal experiments, VPC23109 was diluted into sterile normal saline (NS) and injected at 0.75 mg/kg.

Rodent studies

All murine studies were approved by the Institutional Animal Care and Usage Committee at the Washington University in St. Louis and were preformed following the Guide for the Care and Use of Laboratory Animals. Mice were maintained on a 12:12-hr light-dark schedule in a temperature controlled specific pathogen-free facility and fed standard laboratory mouse chow. Animal procedures were carried out in accordance with the Washington University School of Medicine Animal Studies Committee, which approved the protocols. Blood was obtained from mice by puncturing the right mandibular vein with a 5.5-mm animal lancet and collecting the blood directly into plasma separator tubes kept on ice and centrifuged at 10,000 g for 5 min. Plasma was transferred to cryovials and snap frozen in liquid nitrogen and stored at -80°C. In some experiments urine was also collected and snap frozen in liquid nitrogen. *Apom*^{TG} and *Apom*^{KO} were previously described (18) (15). *Mhc-cre* (42) and *S1pr1*$^{flox/flox}$ (43) mice were purchased from The Jackson Laboratory (Bar Harbor, ME, USA). In age and sex-matched adult mice,

cardiotoxicity was induced by intraperitoneal (IP) injection of doxorubicin at 20 mg/kg for our initial studies with *Apom*^{TG} mice, and 15 mg/kg in *Apom*^{KO} mice studies because of high mortality. Single dose IP injections were also performed with 10 mg/kg. Chronic models utilized 5 mg/kg once weekly x 4 weeks as previously described (11). Echocardiography was performed as previously described, and read blindly by a cardiologist. LV mass and EF were obtained using the Vevostrain package in Vevo (Fujifilm Visualsonics, Toronto, Canada) (30). Leukemic mice were generated by IV injection of male C57Bl/6 (B6; Jackson Laboratory) mice with 5 x 10^5 APL cells (27). After allowing 4 days for engraftment, animals were treated with doxorubicin on days 4, 6, 8, 11, 13, and 15 at 4 mg/kg subcutaneously. On day 17, peripheral blood was obtained via the retroorbital plexus under anesthesia and white blood cell (WBC) counts obtained using an automated cell counter (Hemavet 950, Drew Scientific). The percentage of circulating APL cells in blood was determined by flow cytometry.

Flow cytometry

Erythrocytes were removed from blood samples using ammonium chloride-potassium bicarbonate lysis and WBCs were resuspended in staining buffer (PBS supplemented with 0.5% bovine serum albumin and 2 mM EDTA). Cells were incubated for 30 min at room temperature with pre-titrated saturating dilutions of the following fluorochrome-labeled monoclonal antibodies (BD Biosciences; clone designated in parenthesis): CD45 (104), CD34 (RAM34), CD117 (2B8), and Ly6C (HK1.4). Dead cells were excluded by staining with 2 μg/ml 7-amino-actinomycin D (BD Biosciences) for 5 min prior to analysis. Samples were analyzed on a Gallios flow cytometer (Beckman Coulter) and data were analyzed using FlowJo software (TreeStar, Ashland, OR, USA). APL blasts co-expressed CD34, CD117, and Ly6C.

Histologic analyses

For immunohistochemistry and tissue histology, mid-myocardial tissue was fixed 18-24 hr in 10% formalin, followed by immersion in PBS, then 70% ethanol, and embedded in paraffin. The rest of

the tissues were snap frozen in liquid nitrogen and stored at -80°C. Formalin-fixed paraffin-embedded hearts were used for all immunofluorescence (IF) analyses. Tissue sections were deparaffinized by warming on a 54°C slide warmer for 10 min followed by immersion in xylene at room temperature for 20 min. Rehydration of sections was done by sequential bathing for 5 min each in ethanol solutions progressing from 100%, 95%, 70%, followed by treatment with MaxBlock Autofluorescence Reducing Reagent (Dianova, Berlin, Germany) for 5 min. Sections were rinsed sequentially in 60% ethanol, distilled water, and PBS-tween20 (0.05%). For heat-induced epitope retrieval (HIER), sections were placed in rodent decloaker buffer (RD-913; Bio Care Medical, Concord, CA, USA) and heated at 99°C for 18 min in a pressurized decloaking chamber (Bio Care Medical). At the end of heating, sections remained in the decloaking chamber as it depressurized for 10 min, then removed and allowed to start cooling for 20 min on a bench, and finally placed under a stream of dH_2O for 5 min to fully cool sections and displace the rodent decloaker buffer. Sections were placed in PBS-tween20 for 5 min followed by blocking for 1 hr in normal serum from the same species in which the secondary antibody was raised. After blocking was completed, sections were incubated sequentially in the primary antibody overnight at 4°C, followed by 2 hr in the secondary antibody, and washed in PBS-tween20 for 5 min. Sections were rinsed in dH_2O and treated with MaxBlock Post Detection Conditioner for 5 min. Sections were rinsed in dH_2O and placed in PBS-tween20. This procedure was repeated when a second primary antibody was used. Slides were cover slipped using Vectashield-Plus with DAPI (cat no. H-2000; Vector Labs, Burlingame, CA, USA). Primary antibodies were rabbit anti-LC3 (Novus Biologicals, NB100-2220, 1:200, Littleton, CO, USA), guinea pig anti-p62 (ProGen SAS Technologies, GP62c, 1:200, Delhi, India), rabbit anti-caspase 3 (Cell Signaling, 9662s, 1:400, Danvers, MA, USA), rabbit anti-p-H2AX(ser139) (Cell Signaling, 9718s, 1:200). Secondary antibodies purchased from Life Technologies-Thermo-Fisher (Berkeley, MO, USA) were AF594 donkey anti-rabbit (A21207), and AF488 donkey anti-rabbit (A21206). Secondary antibodies purchased from Jackson Immunoresearch (West Grove, PA, USA) were AF594 donkey anti-guinea pig IgG (cat no. 706-

585-148) and AF488 donkey anti-mouse IgM (cat no. 715-545-140). Confocal images of fluorescent sections were obtained with a Zeiss Axio Imager M2 equipped with a Zeiss LSM 700 laser and a Fujitsu processor. Images were saved as CZVI files using Zen software (Black edition). The images were then quantified using the image analysis module of a digital pathology software Visiomorph (VisioPharm, Broomfield, CO, USA). Masson-trichrome staining was performed as previously described (30). Electron microscopy was performed as previously described (44).

Cell culture

Primary culture of neonatal rat cardiomyocytes (NRCMs) were isolated from the hearts of 1-3 days old Sprague-Dawley (SD) rats (Charles River Labs, Wilmington, MA, USA) and cultured as described previously (45). Briefly, the atria and great vessels were trimmed off, and tissue was finely minced, followed by sequential digestion with 0.5 mg/mL collagenase (Worthington Biochemical, Lakewood, NJ, USA). Ventricular cardiomyocytes were separated from fibroblasts by differential plating and cultured in gelatin-coated tissue culture plates (different plates used depending on the experimental requirements) in medium containing modified Gibco™ Dulbecco's Modified Eagle Medium (DMEM) (Gibco, 11965-084), 10% horse serum (Thermo Fisher, 16050-122), 5% Fetal Bovine Serum (FBS) (Sigma-Aldrich, F2442, St. Louis, MO, USA), 100 µM bromodeoxyuridine (Brdu), 100 U/mL penicillin, 100 µg/mL streptomycin (Thermo Fisher, 15140148) and L-glutamine (Sigma-Aldrich, G8540). NRCMs were serum-starved overnight, then treated with vehicle or FTY720 (Cayman Chemicals, 10006292, Ann Arbor, MI, USA) prior to treating with 0.5 mM doxorubicin for 4 hr. Cells were incubated with 1 µM Lysosensor Yelow/Blue DND 160 (Thermo Fisher, L7545) for 3 min, washed with HCSS and imaged by collecting pairs of images excited at 380 nm and 340 nm (Polychrome V, FEI, Munjch, Germany) through a long pass 480 nm emission filter through a 40x/1.35 oil immersion lens (Olympus) using an iMIC microscope (FEI). After subtracting the matching wavelength

background, the images were divided by each other to yield an excitation ratio images. The ratio values of individual lysosomes were determined using Live Acquisition software package (FEI) and converted to pH using a calibration curve prepared by measuring Lysosensor excitation ratio on calibration buffers of known pH (3.0-6.5) on the same optical system. Human renal proximal tubule epithelial cells were purchased from American Type Culture Collection (ATCC) and cultured in Gibco^{TM} DMEM: Nutrient Mixture F-12 (DMEM/F-12) (Sigma-Aldrich, D8437) supplemented with 5% FBS, 50 µM L-ascorbic-2 phosphate (Sigma-Aldrich, A8960), 0.7% Insulin-Transferrin-Selenium (ITS) (Corning, 25-800-CR), 4 µg/mL Dexamethasone (Sigma-Adlrich, D4902), 10 ng/mL Epidermal Growth Factor human (hEGF) (Sigma-Aldrich, E9644), 1.2 mg/mL $NaHCO_3$ (Sigma-Aldrich, S5761) and 1.5 mM HEPES (Sigma-Aldrich, H4034).

Quantitative Real-Time Polymerase Chain Reaction analysis (qPCR)

Quantitative Real time PCR was performed as described (30). Briefly, total RNA in cardiac tissues and HRPT cells were extracted using RNeasy Mini kit (Qiagen, #74104, Hilden, Germany), and the first-strand cDNA was prepared using the iScriptTM cDNA synthesis kit (Bio-Rad, #1708890, Hercules, CA, USA). qPCR analysis was performed with SYBR Green Master Mix (Bio-Rad, #1725121) on QuantStudio 3 Real-Time PCR system (Applied Biosystems, A28136, Foster City, CA, USA) to examine the relative mRNA levels of indicated genes. Mice sequences for qRT-PCR primers are shown below: ***Apom***: forward 5'-AAC AGA CCT GTT CTC CAG CTC G-3', reverse 5'-GTC CAA GCA AGA GGT CAG AGA C-3'; ***Tfeb***: forward 5'-GTC TAG CAG CCA CCT GAA CGT-3', reverse 5'-ACC ATG GAG GCT GTG ACC TG-3'; ***Actb***: forward 5'-CAG AAG GAG ATC ACT GCC CT-3', reverse 5'-AGT ACT TGC GCT CAG GAG GA-3'; ***36b4***: forward 5'-GCT TCG TGT TCA CCA AGG AGG A-3', reverse 5'-GTC CTA GAC CAG TGT TCT GAG C-3'; ***Rpl32***: forward 5'-CCT CTG GTG AAG CCC AAG ATC-3', reverse 5'-TCT GGG TTT CCG CCA GTT T-3'; ***Gapdh***: forward 5'-ACT CCC ACT CTT CCA CCT TC-3', reverse 5'-TCT TGC TCA GTG TCC TTG C-3'. Human sequences for qRT-PCR primers are

shown below: ***Lrp2***: forward 5'-ATA GAG GGG AGC ACC ACT GA-3', reverse 5'-AGC AAT TTC CTC CGT GCA T-3'; ***Actb***: forward 5'-AGG CCA ACC GCG AGA AG-3', reverse 5'-ACA GCC TGG ATA GCA ACG TAC A-3'; ***36b4***: forward 5'-AAC ATG CTC AAC ATC TCC CC-3', reverse 5'-CCG ACT CCT CCG ACT CTT C-3'; ***Rpl32***: forward 5'-GCC CAA GAT CGT CAA AAA GAG A-3', reverse 5'-TCC GCC AGT TAC GCT TAA TTT-3'; ***Gapdh***: forward 5'-CCA TGT TCG TCA TGG GTG TGA ACC A-3', reverse 5'-GCC AGT AGA GGC AGG GAT GAT GTT G-3'.

Cytoplasm and Nuclear protein extraction

Cardiac tissue were fractionated into nucleus-enriched and cytoplasmic samples by using a CelLytic™ NuCLEAR Extraction kit (Sigma, Nxtract), as previously described (46). Briefly, heart tissue were homogenized in 1x isotonic lysis buffer (ILB) containing 10 mM dithiothreitol (DTT), 1x Proteaase Inhibitor (PI) (Millipore, #4693132001, Burlington, MA, USA) and 1x Halt Protease and Phosphatase Inhibitor (PPI) (Thermo Fisher, #78446) using the Mechanical Homogenizers (IKA, #3737001, Staufen, Germany) and centrifuged at 4°C, 10,500 g for 15 min, and the supernatants were cytoplasmic fraction. The pellets were washed 3 times with 1x ILB and fully resuspended in 1x extraction buffer (EB) containing 10 mM DTT, 1x PI and 1x PPI. The suspension were kept on the ice for 30 min and then completely sonicated by the Sonifier (Branson Ultrasonics, #250-450, Danbury, CT, USA). The supernatant from the 20,500 g spin at 4°C for 5 min were the nuclear fraction. Expression of proteins localized to the nucleus (Histone H3) and cytoplasm (GAPDH) was examined to confirm relative enrichment.

Western blot analysis

Western blot was performed on mice tissue or human samples as previously described (31). In brief, myocardial extracts were prepared by homogenization of ventricular tissue with lysis buffer (composition in mM: 50 Tris HCl, pH 7.4; 2.5 EDTA; 10 EGTA; 20 NaF; 25 $Na_4P_2O_7$.10 H_2O; 2 Na_3VO_4; 25 NaCl) containing 0.2% NP-40, 1x PI and 1x PPI. 15-40 µg of protein were

separated by sodium dodecyl sulfate polyacrylamide gel electrophoresis (SDS-PAGE) (Bio-Rad) and transferred to a polyvinylidene fluoride (PVDF) membrane (Millipore, #3010040001). After being blocked with 5% fat-free milk in TBST, the membranes were incubated with individual primary antibodies overnight at 4°C. Subsequently, the membrane was incubated with a horseradish peroxidase-conjugated secondary antibody (Cell Signaling, #7074 or #7076), and exposed to ClarityTM Western ECL Substrate (Bio-Rad, #170-5060) using the ChemiDoc System (Bio-Rad, 12003153) for detection of protein expression. Primary antibodies employed were as follows: **mouse ApoM** (LS Bio, C158166, diluted 1:1000, Seattle, WA, USA), **human ApoM** (R&D, AF4550, diluted 1:1000, Minneapolis, MN, USA), **TFEB** (Bethyl Labs, A303-673A, diluted 1:1000, Montgomery, TX, USA), **AKT** (Cell Signaling, #9272s, diluted 1:1000), **phospho-AKT(Ser473)** (Cell Signaling, #4060s, diluted 1:2000), **Histone H3** (Cell Signaling, #9715s, diluted 1:1000), **GAPDH** (Abcam, ab22555, diluted 1:5000, Cambridge, MA, USA), **Albumin** (Cell Signaling, #4929s, diluted 1:1000) and **Actin** (Sigma-Aldrich, A2066, diluted 1:4000). The band intensity was measured and analyzed with ImageJ software (Bio-Rad). Urine samples were analyzed by western blot as described (16). The samples (30 µl) were loaded pairwise (pre and post doxorubicin treatment) on 12% SDS-page (Invitrogen, Carlsbad, CA, USA) after addition of reducing agents. As control serial dilution of plasma samples were included. In-house produced rabbit anti-ApoM antibody was used diluted 1:500 as primary antibody (#15297, bleed 5). Secondary antibody was Goat anti-rabbit IgG (Dako, P448) diluted 1:2000. Western blots were analyzed using an Odyssey® instrument (LI-COR Biosciences, Lincoln, NE, USA).

Insoluble protein isolation

Insoluble protein isolation was performed as previously described (30). Heart tissue was mechanically homogenized with a Dounce homogenizer in 500-1000ul of homogenization buffer (0.3 M KCl, 0.1 M KH_2PO_4, 50 mM K_2HPO_4, 10 mM EDTA, 4 mM Na Orthovanadate, 100

mM NaF, Protease inhibitor, pH to 6.5). Homogenized samples were passed through mesh basket on ice, followed by collection of the lysate run-through which was incubated on ice for 30 min. A known volume of the sample was transferred to another Eppendorf tube and 20% NP-40 was added to for a final concentration of 1% NP-40. Samples were then incubated on ice for 30 min, and spun at 20,500 g for 15 min, 4°C. Supernatant was collected as soluble fraction. The pellet was washed 3 times with cold PBS (following addition of 1ml PBS to each pellet, and spin down at 20,500 g for 10 min) followed by resuspension in 1% SDS, 10 mM Tris buffer to generate the insoluble fraction.

Human samples and ApoM determination

For circulating ApoM protein determination, patients > 18 years of age diagnosed with HER2-positive breast cancer and scheduled to receive adjuvant therapy (anthracyclines, taxanes, and trastuzumab) were recruited prospectively and consecutively from Massachusetts General Hospital, MD Anderson Cancer Center, and McGill University (47, 48). The study was approved by the institutional review board of the participating institutions, and all subjects gave informed consent. The typical cancer treatment regimen consisted of doxorubicin 60 mg/m^2 and cyclophosphamide 600 mg/m^2 every 3 weeks for 4 cycles. At 3 months, all patients received paclitaxel 80 mg/m^2 and trastuzumab 2 mg/kg weekly for 12 weeks, followed by trastuzumab 6 mg/kg every 3 weeks for 1 year. ApoM was measured in plasma samples using the SomaScan aptamer-based proteomics platform, as previously described and validated (23, 49, 50). For assessment of insoluble p62 in the human myocardium, deidentified human heart tissue samples were obtained from the Human Heart Tissue Bank at the University of Pennsylvania as previously described (51). Transmural LV samples from non-failing donors (obtained from brain-dead donors with no clinical history of HF) or anthracycline-induced cardiomyopathy (obtained at time of orthotopic heart transplantation) were obtained from the LV free wall, with epicardial fat excluded, and flash frozen in liquid nitrogen.

Statistical analyses

All data are presented as Mean ± SEM and analyzed by Graphpad Prism 9.0. The statistical comparisons between two groups were analyzed by unpaired Student's t test. The statistical significance among multiple groups was analyzed by analysis of variance (ANOVA) and multiple testing corrections, as specified in each figure legend. In all of the analyses, a value of $P < 0.05$ was considered statistically significant.

Study approval

All animal studies were approved by the Animal Studies Committee at Washington University School of Medicine. Human studies were deemed exempt by the Washington University School of Medicine due to the fact that only de-identified human samples were utilized.

Author Contributions

ZG contributed to writing the manuscript, conception and design of the experiments, and performed experiments. AP, CVR, EC, AG, TR, HE, JVT, AK, KH, SVS performed experiments and assisted with writing the manuscript. XM provided technical assistance and critically reviewed the manuscript. AA, MSC and KBM provided human data, and critically reviewed the manuscript. CC performed experiments and critically reviewed the manuscript. AD and JSP provided critical reagents and critically reviewed the manuscript. LAC, MPR, JFD critically reviewed the manuscript. AJ designed experiments and wrote the manuscript.

Acknowledgements

AJ was supported by K08HL138262 from the NHLBI and by the Diabetes Research Center at Washington University in St. Louis of the National Institutes of Health under award number P30DK020579, as well as the NIH grant P30DK056341 (Nutrition Obesity Research Center). AD was supported by grants from the Department of Veterans Affairs (I01BX004235) and the National Institutes of Health (HL107594). MSC is supported by R01HL130539 and

R01HL131613. Research reported in this publication was also supported by the National Cancer Institute of the National Institutes of Health under Award Number R50CA211466 (MPR), R35CA210084 (JFD), P01CA101937 (JFD) and R01HL119962 (JSP). We thank technician Charlotte Wandel for excellent assistant with western blot analysis of urine. We acknowledge support from the NIH Shared Instrumentation Grant (S10RR027552) for support through the Hope Center Neuroimaging Core, the Molecular Microbiology Imaging Facility, and the Advanced Imaging and Tissue Analysis Core of the Digestive Disease Research Core Center (DDRCC NIH P30DK052574) at Washington University School of Medicine.

References

1. Sturgeon KM, et al. A population-based study of cardiovascular disease mortality risk in US cancer patients. *Eur Heart J.* 2019;40(48):3889-97.
2. Armenian S, and Bhatia S. Predicting and Preventing Anthracycline-Related Cardiotoxicity. *Am Soc Clin Oncol Educ Book.* 2018;38:3-12.
3. Lipshultz SE, et al. Late cardiac effects of doxorubicin therapy for acute lymphoblastic leukemia in childhood. *N Engl J Med.* 1991;324(12):808-15.
4. Neilan TG, et al. Left ventricular mass in patients with a cardiomyopathy after treatment with anthracyclines. *Am J Cardiol.* 2012;110(11):1679-86.
5. Jordan JH, et al. Left Ventricular Mass Change After Anthracycline Chemotherapy. *Circ Heart Fail.* 2018;11(7):e004560.
6. Nadruz W, et al. Cardiovascular phenotype and prognosis of patients with heart failure induced by cancer therapy. *Heart.* 2019;105(1):34-41.
7. Hardaway BW. Adriamycin-associated cardiomyopathy: where are we now? updates in pathophysiology, dose recommendations, prognosis, and outcomes. *Curr Opin Cardiol.* 2019;34(3):289-95.
8. Fornaro A, et al. Comparison of long-term outcome in anthracycline-related versus idiopathic dilated cardiomyopathy: a single centre experience. *Eur J Heart Fail.* 2018;20(5):898-906.
9. Zhang S, et al. Identification of the molecular basis of doxorubicin-induced cardiotoxicity. *Nat Med.* 2012;18(11):1639-42.
10. Ichikawa Y, et al. Cardiotoxicity of doxorubicin is mediated through mitochondrial iron accumulation. *J Clin Invest.* 2014;124(2):617-30.
11. Li DL, et al. Doxorubicin Blocks Cardiomyocyte Autophagic Flux by Inhibiting Lysosome Acidification. *Circulation.* 2016;133(17):1668-87.

12. Bartlett JJ, et al. Doxorubicin impairs cardiomyocyte viability by suppressing transcription factor EB expression and disrupting autophagy. *Biochem J.* 2016;473(21):3769-89.

13. Durham KK, et al. Treatment with apolipoprotein A1 protects mice against doxorubicin-induced cardiotoxicity in a scavenger receptor class B, type I-dependent manner. *Am J Physiol Heart Circ Physiol.* 2019;316(6):H1447-H57.

14. Frias MA, et al. Native and reconstituted HDL protect cardiomyocytes from doxorubicin-induced apoptosis. *Cardiovasc Res.* 2010;85(1):118-26.

15. Christoffersen C, et al. Endothelium-protective sphingosine-1-phosphate provided by HDL-associated apolipoprotein M. *Proc Natl Acad Sci U S A.* 2011;108(23):9613-8.

16. Christoffersen C, et al. Isolation and characterization of human apolipoprotein M-containing lipoproteins. *J Lipid Res.* 2006;47(8):1833-43.

17. Xu N, and Dahlback B. A novel human apolipoprotein (apoM). *The Journal of biological chemistry.* 1999;274(44):31286-90.

18. Liu M, et al. Hepatic apolipoprotein M (apoM) overexpression stimulates formation of larger apoM/sphingosine 1-phosphate-enriched plasma high density lipoprotein. *The Journal of biological chemistry.* 2014;289(5):2801-14.

19. Elsoe S, et al. Apolipoprotein M binds oxidized phospholipids and increases the antioxidant effect of HDL. *Atherosclerosis.* 2012;221(1):91-7.

20. Christoffersen C, et al. Effect of apolipoprotein M on high density lipoprotein metabolism and atherosclerosis in low density lipoprotein receptor knock-out mice. *The Journal of biological chemistry.* 2008;283(4):1839-47.

21. Christensen PM, et al. Impaired endothelial barrier function in apolipoprotein M-deficient mice is dependent on sphingosine-1-phosphate receptor 1. *FASEB J.* 2016;30(6):2351-9.

22. Ruiz M, Okada H, and Dahlback B. HDL-associated ApoM is anti-apoptotic by delivering sphingosine 1-phosphate to S1P1 & S1P3 receptors on vascular endothelium. *Lipids Health Dis.* 2017;16(1):36.

23. Chirinos JA, et al. Reduced Apolipoprotein M and Adverse Outcomes Across the Spectrum of Human Heart Failure. *Circulation.* 2020.

24. Cardinale D, et al. Early detection of anthracycline cardiotoxicity and improvement with heart failure therapy. *Circulation.* 2015;131(22):1981-8.

25. Faber K, et al. Megalin is a receptor for apolipoprotein M, and kidney-specific megalin-deficiency confers urinary excretion of apolipoprotein M. *Mol Endocrinol.* 2006;20(1):212-8.

26. Nervi B, et al. Chemosensitization of acute myeloid leukemia (AML) following mobilization by the CXCR4 antagonist AMD3100. *Blood.* 2009;113(24):6206-14.

27. Westervelt P, et al. High-penetrance mouse model of acute promyelocytic leukemia with very low levels of PML-RARalpha expression. *Blood.* 2003;102(5):1857-65.

28. Kao J, et al. gamma-H2AX as a therapeutic target for improving the efficacy of radiation therapy. *Curr Cancer Drug Targets.* 2006;6(3):197-205.

29. Javaheri A, et al. TFEB activation in macrophages attenuates postmyocardial infarction ventricular dysfunction independently of ATG5-mediated autophagy. *JCI Insight.* 2019;4(21).

30. Ma X, et al. Transcription Factor EB Activation Rescues Advanced alphaB-Crystallin Mutation-Induced Cardiomyopathy by Normalizing Desmin Localization. *J Am Heart Assoc.* 2019;8(4):e010866.

31. Hartupee J, et al. Impaired Protein Quality Control During Left Ventricular Remodeling in Mice With Cardiac Restricted Overexpression of Tumor Necrosis Factor. *Circ Heart Fail.* 2017;10(12).

32. Chen YZ, et al. Sphingosine 1 phosphate receptor-1 (S1PR1) signaling protects cardiac function by inhibiting cardiomyocyte autophagy. *J Geriatr Cardiol.* 2018;15(5):334-45.

33. Keul P, et al. Sphingosine-1-Phosphate Receptor 1 Regulates Cardiac Function by Modulating Ca2+ Sensitivity and Na+/H+ Exchange and Mediates Protection by Ischemic Preconditioning. *J Am Heart Assoc.* 2016;5(5).

34. Kurano M, et al. Apolipoprotein M Protects Lipopolysaccharide-Treated Mice from Death and Organ Injury. *Thromb Haemost.* 2018;118(6):1021-35.

35. Zhitomirsky B, and Assaraf YG. Lysosomal accumulation of anticancer drugs triggers lysosomal exocytosis. *Oncotarget.* 2017;8(28):45117-32.

36. Theilmeier G, et al. High-density lipoproteins and their constituent, sphingosine-1-phosphate, directly protect the heart against ischemia/reperfusion injury in vivo via the S1P3 lysophospholipid receptor. *Circulation.* 2006;114(13):1403-9.

37. Swendeman SL, et al. An engineered S1P chaperone attenuates hypertension and ischemic injury. *Sci Signal.* 2017;10(492).

38. Malik FA, et al. Sphingosine-1-Phosphate Is a Novel Regulator of Cystic Fibrosis Transmembrane Conductance Regulator (CFTR) Activity. *PLoS One.* 2015;10(6):e0130313.

39. Collodet C, et al. AMPK promotes induction of the tumor suppressor FLCN through activation of TFEB independently of mTOR. *FASEB J.* 2019;33(11):12374-91.

40. Mani K, Javaheri A, and Diwan A. Lysosomes Mediate Benefits of Intermittent Fasting in Cardiometabolic Disease: The Janitor Is the Undercover Boss. *Compr Physiol.* 2018;8(4):1639-67.

41. Hunter WG, et al. High-Density Lipoprotein Particle Subfractions in Heart Failure With Preserved or Reduced Ejection Fraction. *J Am Coll Cardiol.* 2019;73(2):177-86.

42. Agah R, et al. Gene recombination in postmitotic cells. Targeted expression of Cre recombinase provokes cardiac-restricted, site-specific rearrangement in adult ventricular muscle in vivo. *J Clin Invest.* 1997;100(1):169-79.

43. Allende ML, Yamashita T, and Proia RL. G-protein-coupled receptor S1P1 acts within endothelial cells to regulate vascular maturation. *Blood.* 2003;102(10):3665-7.

44. Liu H, et al. Intermittent fasting preserves beta-cell mass in obesity-induced diabetes via the autophagy-lysosome pathway. *Autophagy.* 2017;13(11):1952-68.

45. Ma X, et al. Impaired autophagosome clearance contributes to cardiomyocyte death in ischemia/reperfusion injury. *Circulation.* 2012;125(25):3170-81.

46. Ma X, et al. Regulation of the transcription factor EB-PGC1alpha axis by beclin-1 controls mitochondrial quality and cardiomyocyte death under stress. *Mol Cell Biol.* 2015;35(6):956-76.

47. Sawaya H, et al. Assessment of echocardiography and biomarkers for the extended prediction of cardiotoxicity in patients treated with anthracyclines, taxanes, and trastuzumab. *Circ Cardiovasc Imaging.* 2012;5(5):596-603.

48. Ky B, et al. Early increases in multiple biomarkers predict subsequent cardiotoxicity in patients with breast cancer treated with doxorubicin, taxanes, and trastuzumab. *J Am Coll Cardiol.* 2014;63(8):809-16.

49. Ngo D, et al. Aptamer-Based Proteomic Profiling Reveals Novel Candidate Biomarkers and Pathways in Cardiovascular Disease. *Circulation.* 2016;134(4):270-85.

50. Mosley JD, et al. Probing the Virtual Proteome to Identify Novel Disease Biomarkers. *Circulation.* 2018;138(22):2469-81.

51. Bedi KC, Jr., et al. Evidence for Intramyocardial Disruption of Lipid Metabolism and Increased Myocardial Ketone Utilization in Advanced Human Heart Failure. *Circulation.* 2016;133(8):706-16.

Figure 1

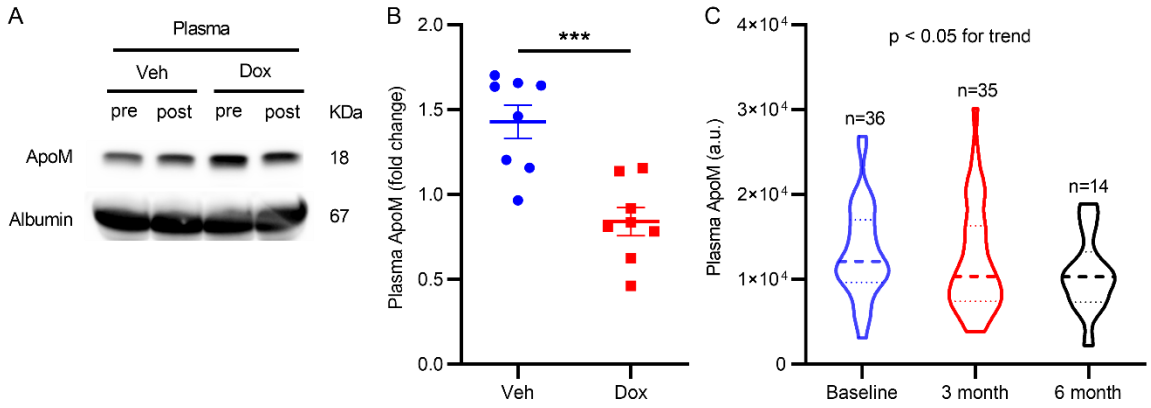

Figure 1. Anthracyclines reduce circulating ApoM protein levels.

A) Representative western blot for ApoM from plasma isolated from mice 48 hr after treatment with vehicle (Veh) or 10 mg/kg doxorubicin (Dox) IP. **B)** Quantification of (A), Student's t-test, n=8 per group. Each dot represents one mouse. **C)** Aptamer-based ApoM plasma levels in patients with breast cancer after 4 cycles of anthracycline. Mixed-effects model, n=36 at baseline, 35 at 3 months, 14 at 6 months. Dotted lines represent median and quartiles. ***p < 0.001.

Figure 2

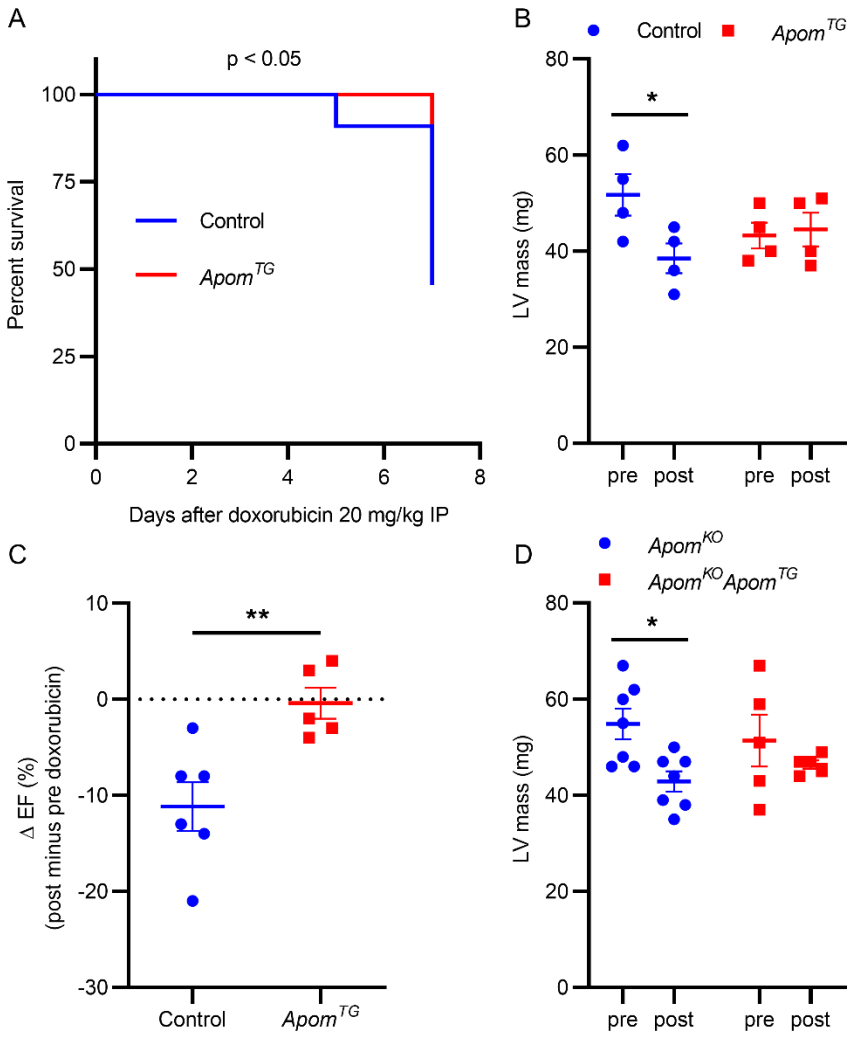

Figure 2. ***Apom*^{TG} attenuates murine doxorubicin cardiotoxicity.**

A) Survival of littermate control and *Apom*^{TG} mice after 20 mg/kg doxorubicin (Dox) IP, n=11 controls vs n=9 *Apom*^{TG}, log-rank test. **B)** Change in LV mass from baseline and 5 days after 20 mg/kg doxorubicin. Two-way repeated measures ANOVA with Sidak correction for multiple comparisons, n=4 per group. **C)** Change in LVEF 3 months after 4 weekly doses of 5 mg/kg doxorubicin IV. Student's t-test, n=6 control vs n=5 *Apom*^{TG}. **D)** LV mass at baseline and 5 days after 15 mg/kg doxorubicin. Two-way repeated measures ANOVA with Sidak correction for multiple comparisons, n=7 *Apom*^{KO} vs n=5 *Apom*^{KO} *Apom*^{TG}. Each dot represents one mouse. *p < 0.05, **p < 0.01.

Figure 3

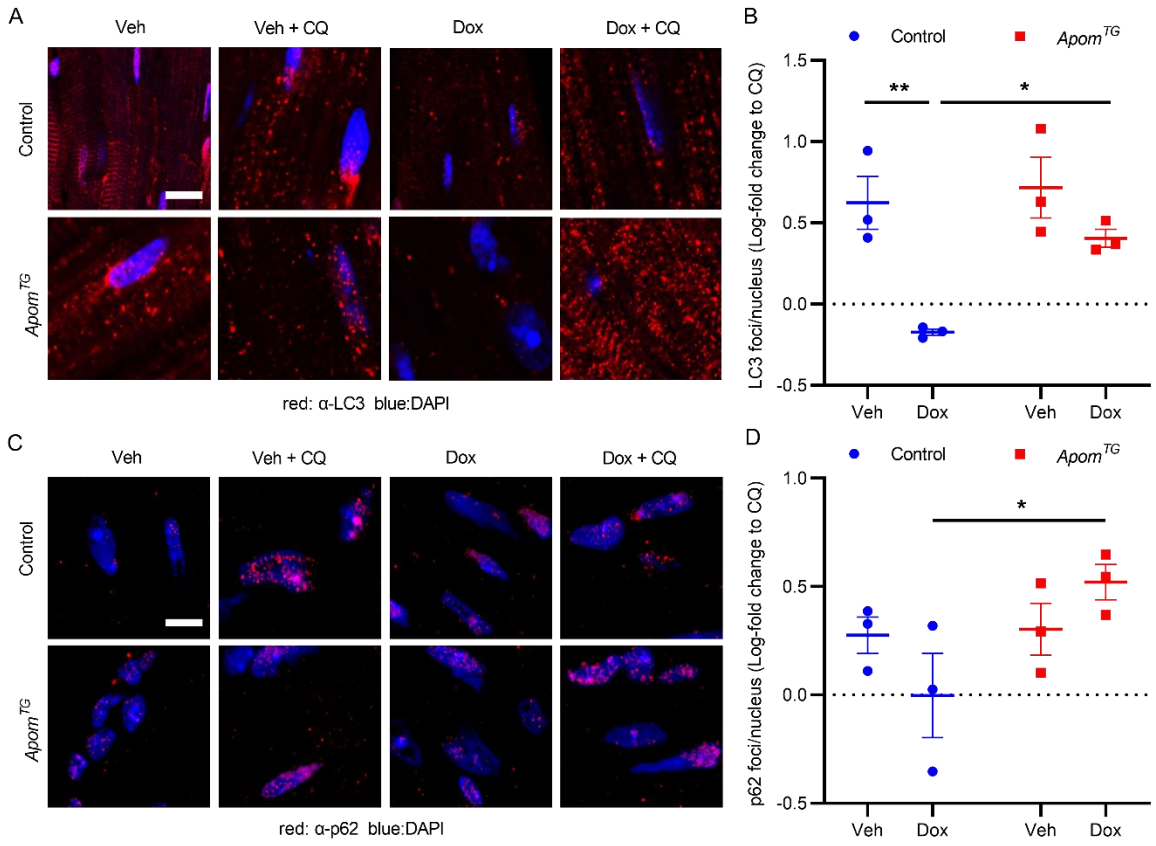

Figure 3. ApoM attenuates doxorubicin-induced autophagic impairment.

A) Representative images of immunohistochemical staining of mid-myocardial sections with α-LC3 and DAPI in littermate control and *Apom*^{TG} mice 48 hr post-treatment with vehicle (Veh) or doxorubicin (Dox, 10 mg/kg) IP and, 4 hr prior to euthanasia, with vehicle vs chloroquine (CQ, 60 mg/kg) IP, scale bar=20 μm. **B)** Blinded quantification of LC3 foci. Two-way ANOVA with Sidak correction for multiple comparisons, n=3 per group. Data were log transformed due to violation of normality. **C)** Representative images immunohistochemical staining of mid-myocardial sections with α-p62 and DAPI in mice from (A), scale bar=20 μm. **D)** Blinded quantification of p62 foci. Two-way ANOVA with Sidak correction for multiple comparisons, n=3 per group. Data were log transformed due to violation of normality. Each dot represents one mouse. *$p < 0.05$, **$p < 0.01$.

Figure 4

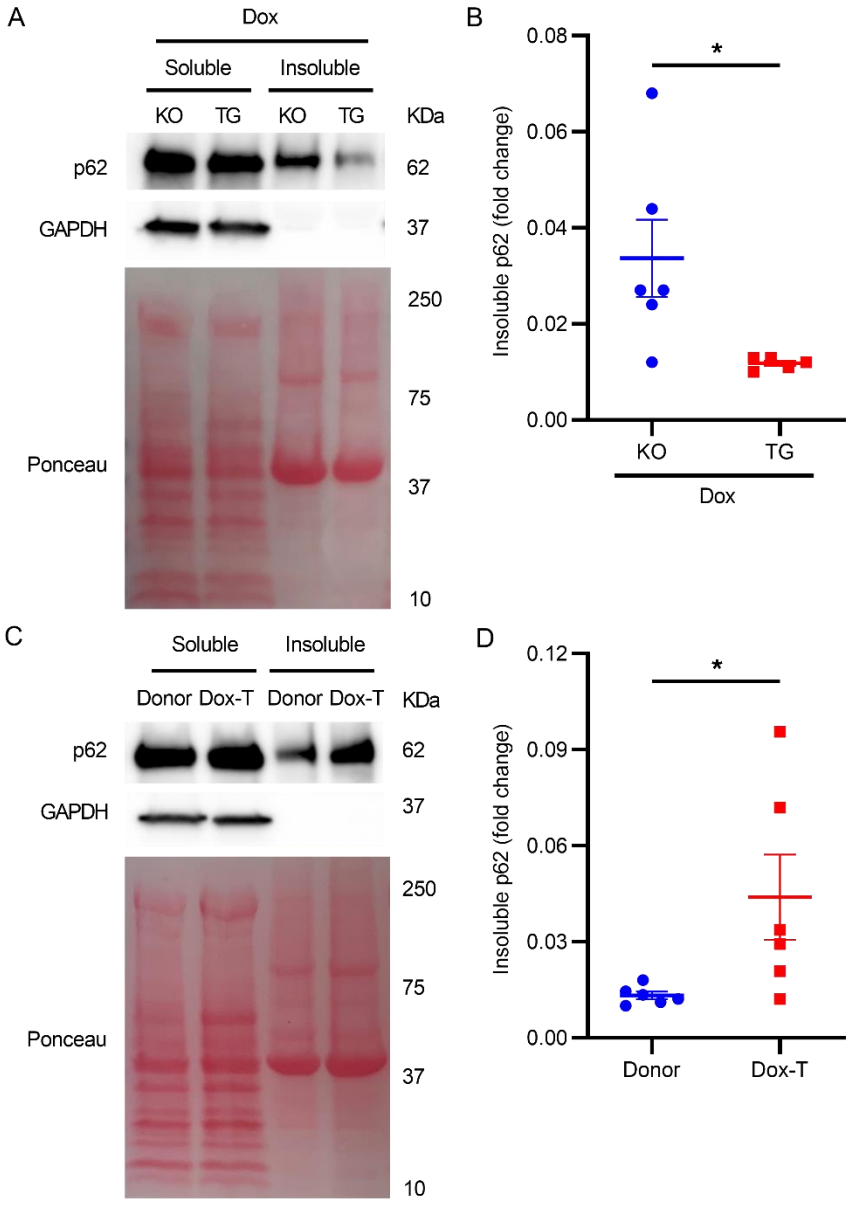

Figure 4. Insoluble p62 protein levels are suppressed by ApoM but elevated in human anthracycline cardiomyopathy.

A) Representative western blot for myocardial soluble vs insoluble p62 from *Apom*^{KO} (KO) and *Apom*^{KO} *Apom*^{TG} (TG) mice 5 days after 15 mg/kg doxorubicin (Dox) IP. **B)** Insoluble p62 quantified relative to soluble p62. Student's t-test, n=6 *Apom*^{KO} vs n=5 *Apom*^{KO} *Apom*^{TG}. Each dot represents one mouse. **C)** Representative western blot for myocardial soluble vs insoluble

p62 from patients with a history of heart failure due to anthracycline cardiomyopathy (Dox-T) versus donor controls (Donor) obtained from patients without any known clinical heart failure. **D)** Insoluble p62 quantified relative to soluble p62. Student's t-test, n=6 per group. Each dot represents one patient. *p < 0.05.

Figure 5

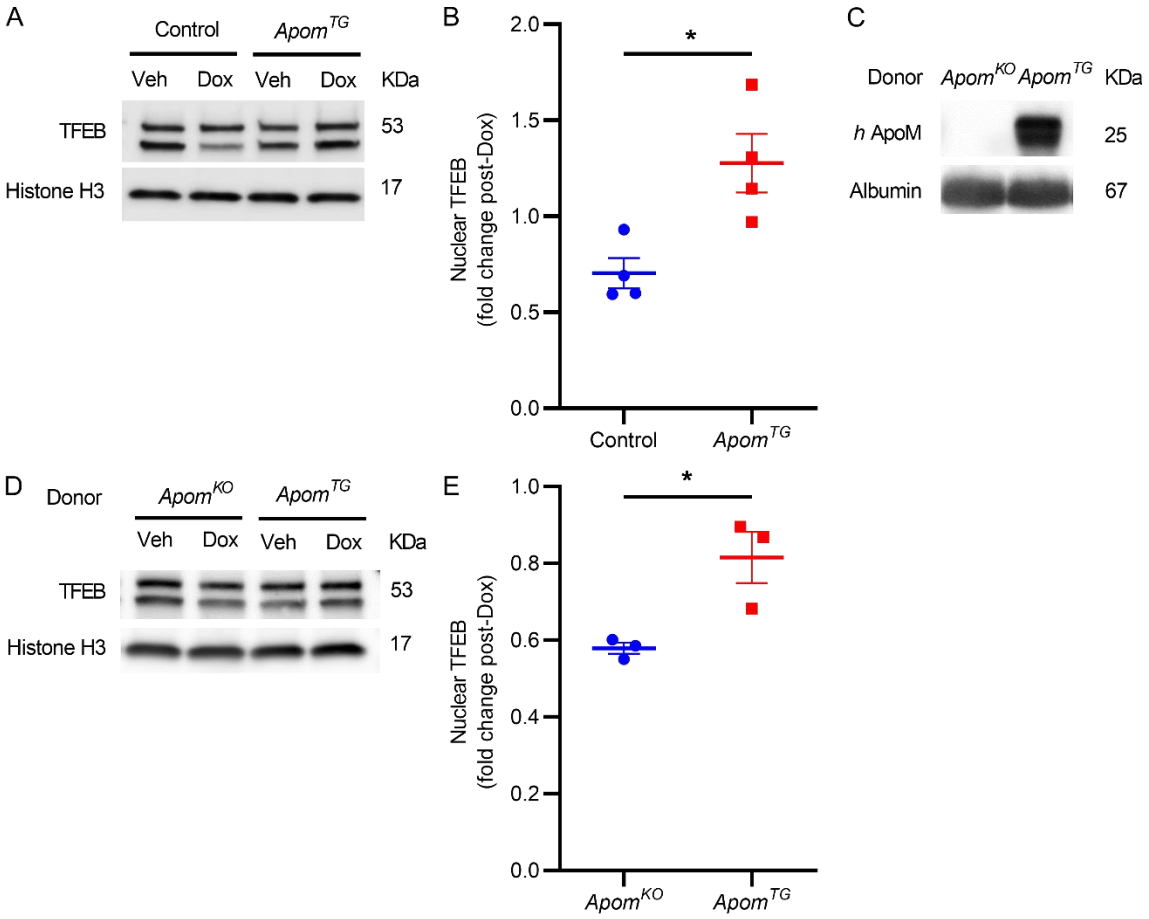

Figure 5. ApoM attenuates doxorubicin-induced reductions in nuclear TFEB.

A) Representative western blot of TFEB from isolated myocardial nuclear protein extracts from littermate control and *Apom*^{TG} mice 48 hr after treatment with vehicle (Veh) or doxorubicin (Dox, 10 mg/kg) IP. **B)** Graph of fold change in nuclear TFEB from (A). Student's t-test, n=4 per group. **C)** Representative western blot of human ApoM from plasma obtained from *Apom*^{KO} mice 2 days after transfer of 120 µL plasma obtained from *Apom*^{KO} or *Apom*^{TG} donor mice. **D)** Representative western blot of myocardial nuclear TFEB in mice from (C) treated with vehicle or doxorubicin (2 days, 10 mg/kg) IP. **E)** Graph of fold change in nuclear TFEB from (D). Student's t-test, n=3 per group. Each dot represents one mouse. *p < 0.05.

Figure 6

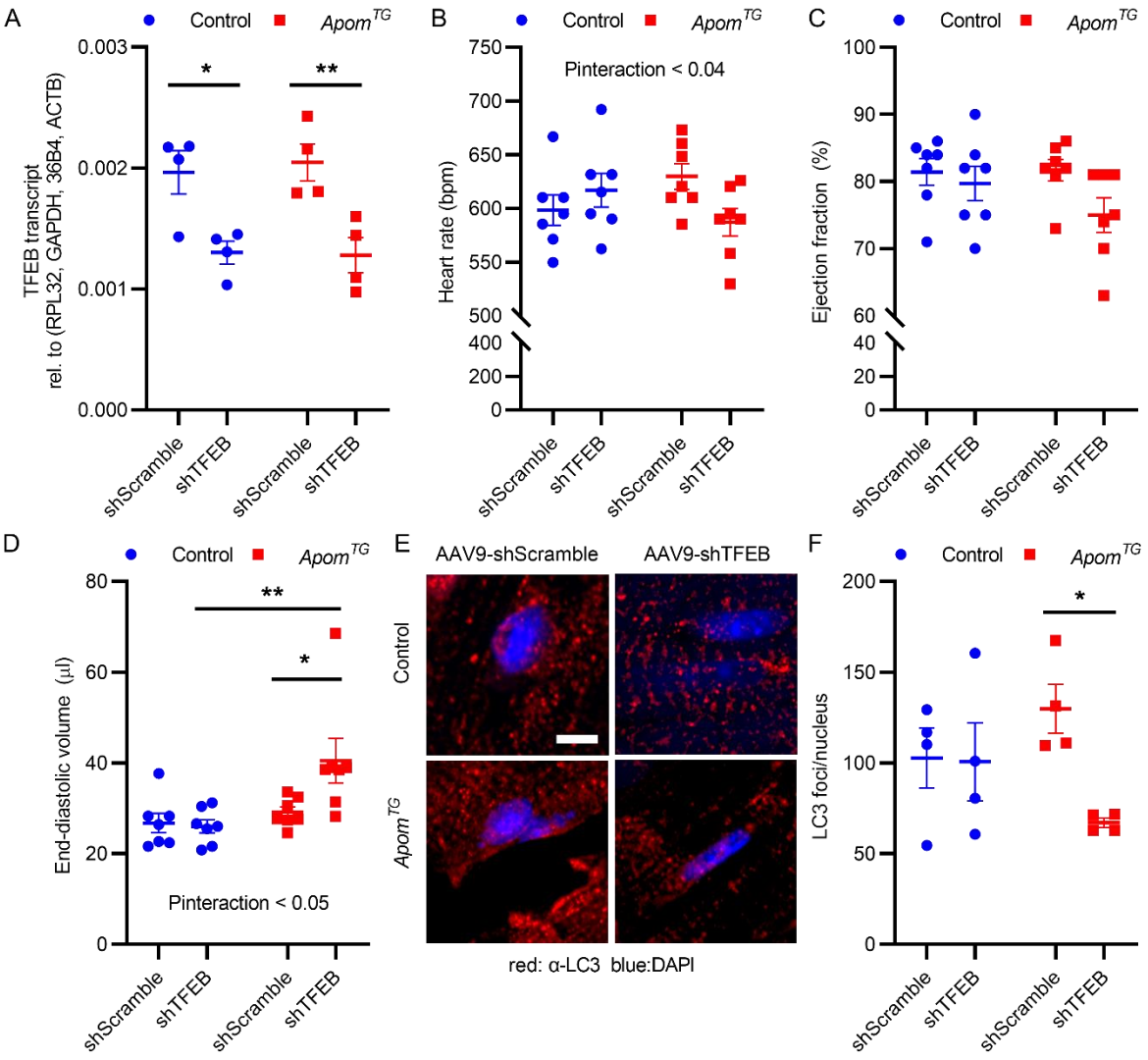

Figure 6. TFEB knockdown provokes cardiomyopathy in *Apom^{TG}* mice.

A) TFEB mRNA abundance accessed by qPCR in littermate control and *Apom^{TG}* mice transduced with AAV9-shScramble or AAV9-shTFEB. Two-way ANOVA with Sidak correction for multiple comparisons, n=4 per group. **B-D)** Heart rate, ejection fraction, and end-diastolic volume assessed by echocardiography 2 weeks after viral transduction. Two-way ANOVA with Sidak correction for multiple comparisons, n=7 per group. **E)** Representative images of immunohistochemical assessment of LC3 foci in myocardial sections, scare bar=5 µm. **F)**

Blinded quantification of LC3 foci from (E). Two-way ANOVA with Sidak correction for multiple comparisons, n=4 per group. Each dot represents one mouse. *$p < 0.05$, **$p < 0.01$.

Figure 7

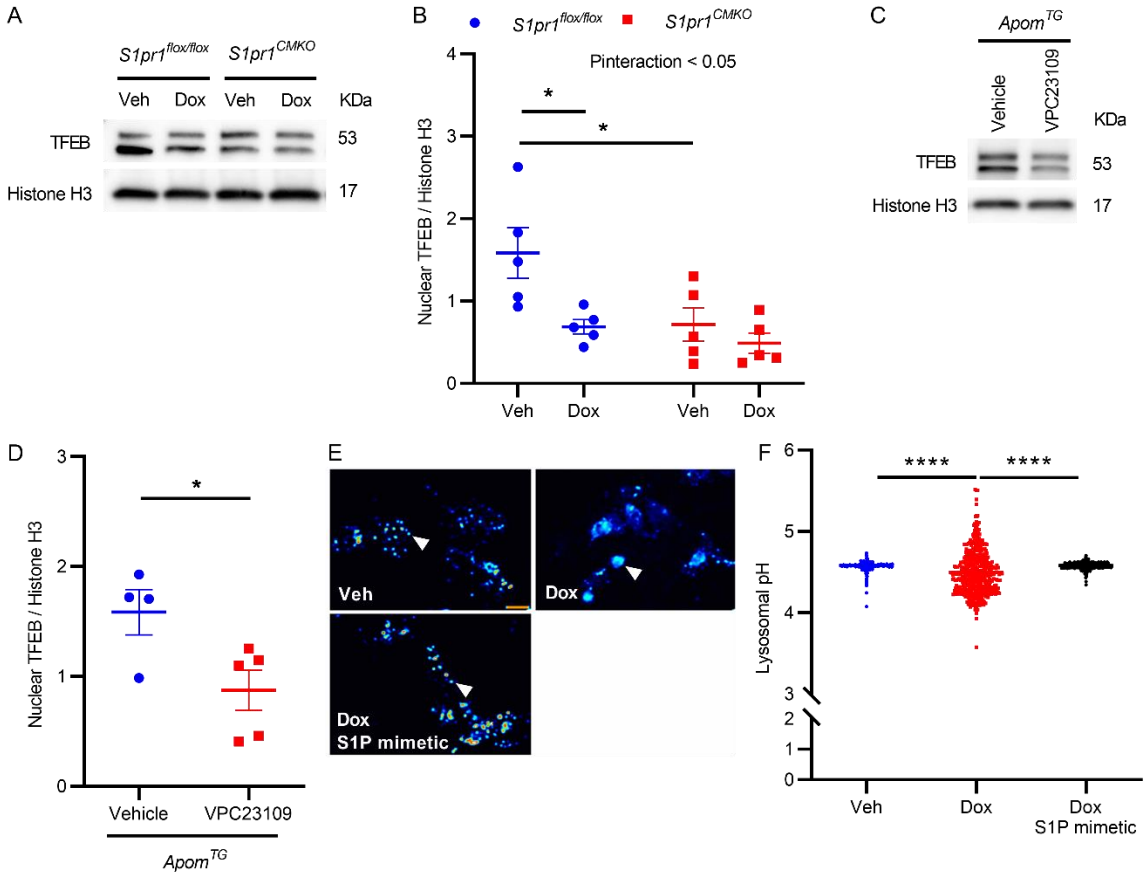

Figure 7. Cardiomyocyte S1P signaling through S1PR1 regulates myocardial TFEB.

A) Representative western blot for myocardial, nuclear TFEB from *S1pr1*$^{flox/flox}$ and *Mhc-cre S1pr1*$^{flox/flox}$ (*S1pr1*^{CMKO}) mice 48 hr after vehicle (Veh) or doxorubicin (Dox, 10 mg/kg) IP. **B)** Graph of fold change in nuclear TFEB from (A). Two-way ANOVA with Sidak correction for multiple comparisons, n=5 per group. Each dot represents one mouse. **C)** Representative western blot of myocardial, nuclear TFEB from *Apom*^{TG} mice treated with vehicle or the S1P receptor inhibitor VPC23109 (0.75 mg/kg, IP daily x 3 days). **D)** Graph of fold change in nuclear TFEB from (C). Student's t-test, n=4 vehicle vs n=5 VPC23109. Each dot represents one mouse. **E)** S1P mimetic pre-treatment of neonatal rat cardiomyocytes attenuates lysosomal injury. Representative pseudocolor excitation ratio images of Lysosensor-loaded lysosomes in cells exposed to DMSO, 0.5 µM Dox and 0.5 µM Dox with 25 nM FTY720 pre-treatment for 5

min. Cells were incubated with 1 µM Lysosensor Yelow/Blue DND 160 for 3 min, washed with HCSS and imaged by collecting pairs of images excited at 380 nm and 340 nm through a long pass 480 nm emission filter through a 40 x /1.35 oil immersion lens (Olympus). Frequency distribution of the excitation ratio values in single lysosomes, scale bar=25 µm. White arrow indicates lysosome. **F)** Graph of lysosomal pH from (E) and data for individual lysosomes pooled from 3 separate litters of rats were collected in 30-60 individual cells. One-way ANOVA with multiple comparisons. Each dot represents one lysosome. *$p < 0.05$, ****$p < 0.0001$.

Graphical Abstract